Viscoelastic normal indentation of nominally flat randomly rough contacts

A. Papangelo[1,2,*], M. Ciavarella[1,2]

(1) *Politecnico di Bari, Department of Mechanics Mathematics and Management, Via Orabona 4, 70125 Bari.*

(2) *Hamburg University of Technology, Department of Mechanical Engineering, Am Schwarzenberg-Campus 1, 21073 Hamburg, Germany*

email: antonio.papangelo@poliba.it

Abstract

Viscoelastic materials are receiving increasing attention in soft robots and pressure sensitive adhesives design, but also in passive damping techniques in automotive and aerospace industry. Here, by using the correspondence principle originally developed by Lee and Radok and further extended by Ting and Greenwood, we transform the elastic solutions of Persson for contact of nominally flat but randomly rough surfaces to viscoelastic indentation. As an example, the cases of step loading and of the response to a single cycle of harmonic loading are studied. For the latter, the effect of the loading frequency, of the ratio between the rubbery and the glassy moduli of the material, and of the mean normal load on the dissipated energy per cycle is studied in detail for a standard viscoelastic material. The results shown are significant for the engineering applications involving cyclic indentation of soft materials, such as in tire-road contact, seals, pick-and-place manipulators and grippers.

Keywords:
Viscoelasticity, dissipation, rough surfaces, contact mechanics, Persson solution

1. Introduction

Soft polymeric material are attracting more and more attention as they are playing a key role in key technological sectors, such as human-robot interaction [1], soft manipulators [2], viscoelastic dampers [3][4][5][6], pressure-

sensitive adhesives [8]. Those materials are known to be viscoelastic, i.e. their mechanical properties depend on the excitation frequency, which gives rise to viscoelastic effects that are fundamental to the understanding of friction [9][10][11][12][13] and adhesion [14], as well as in vibration control of mechanical components through dampers, widely used in the automotive and aerospace industry to reduce noise and vibration and have a better interior sound quality [3][4][5][6][7].

Several research groups are paying their attention to understand how frictional resistance and adhesion interact [15, 16, 17, 18, 19, 20]. Frictional sliding tests with polymeric slab (similarly to what happens in tire-road contact) have reveled that rubber friction has two peaks [21, 22], one usually attributed to adhesion (at low sliding speed) an the other due to viscoelastic losses (at high speed) [23, 24, 25, 26, 21]. Despite the great effort spent to model [17, 15, 16, 19, 20], simulate [20, 27] and test soft materials [15, 16, 18, 28, 29], predictive models are still out of reach, particularly because of the multiscale nature of the contact interface, hence numerical techniques [30, 31, 32] or direct measurements via costly experimental campaigns have to be performed [33].

For rough elastic contacts, understanding the dependence of the real contact area on the squeezing pressure has been understood as a fundamental problem of tribology as it was speculated that the frictional resistance to the relative motion of two sliding objects was proportional to the real contact area [34, 35, 36]. Indeed, recent experimental results involving transparent polymeric materials in contact have shown that the inception of slip is accompanied with the rupture fronts propagating at the interface [37, 38], which significantly reduce the area of intimate contact. It was shown that the inception of slip can be accurately interpreted using fracture mechanics concepts [39, 40]. Hence, understanding how the interfacial roughness influences the variation of the real contact area is of great importance and for this it has received a great attention from the scientific community [41, 42, 43, 44, 45]. The problem has been tackled both from a theoretical point of view [36, 46, 47, 48, 49] or using numerical approaches [41, 44, 45, 50, 51, 52]. Numerical techniques usually exploit the finite element [50, 52, 58] or the boundary element [53, 54, 55, 56, 57] method and can more easily account for realistic boundary conditions or nonlinearities (e.g. large deformations, plasticity [50, 52]). On the other hand numerical techniques are limited to a certain number of degrees of freedom that can be simulated [44], which translates in a finite dimension of the physical domain that can

be solved in a reasonable time. From this point of view analytical techniques are certainly superior as they are able to account also wide surface spectrum with very low computational effort and easily showing the parametric and functional dependence of the solution sought [36, 46, 47, 48, 49].

For elastic contacts, the dependence of the real contact area and of the average interfacial separation on the squeezing pressure has been solved in detail by Persson and coauthors [47, 48, 49], nevertheless a clear understanding of the role of material viscoelasticity in normal indentation has not been addressed yet. A rigorous solution by Lee and Radok [59] permits to obtain viscoelastic results from known results of elastic contact under certain restrictions, and we shall try to concentrate here on the problem of viscoelastic indentation between bodies of nominally flat surfaces with random roughness (Fig. 1), for which Persson and his collaborators [47, 48, 49] have given accurate solutions. Indeed, we shall transform Persson's solution for contact mechanics between rough bodies to viscoelastic contact, using the method of Lee and Radok [59], further developed by Ting [60] and Greenwood [61] for the case when the contact area is decreasing.

Lee and Radok method [59] (and its extensions [60, 61]) has been rigorously derived for simply connected contact area, while we will make the approximation of using it even for rough contact, which clearly involves several contact patches. However, there are good reasons to believe the solution we will provide is a good approximation of the real one (which should be obtained numerically). Indeed, in partial contact, the geometry is not too far from that of a set of independent spherical (Hertzian) contacts. Furthermore, Lee and Radok [59] showed that their solution is not limited to axisymmetric contacts, but can be applied to any quadratic profile, also with differing principal radii of curvature. The latter is an assumption commonly used to reduce a rough surface to a set of asperities, since the seminal work of Bush et al. [46]. Moreover, in full contact, the problem is essentially linear and the correspondence principle is probably trivially valid.

The manuscript is organized as follows: in Section 2 the fundamental results of Persson theories for nominally flat randomly rough contacts are recalled; in Section 3 the viscoelastic solution is derived and exemplary results are shown for the cases of pressure and displacement step loading; in Section 4 the case of harmonic pressure loading is considered and the viscoelastic dissipation is computed for the first loading cycle; in Section 5 the conclusion are drawn.

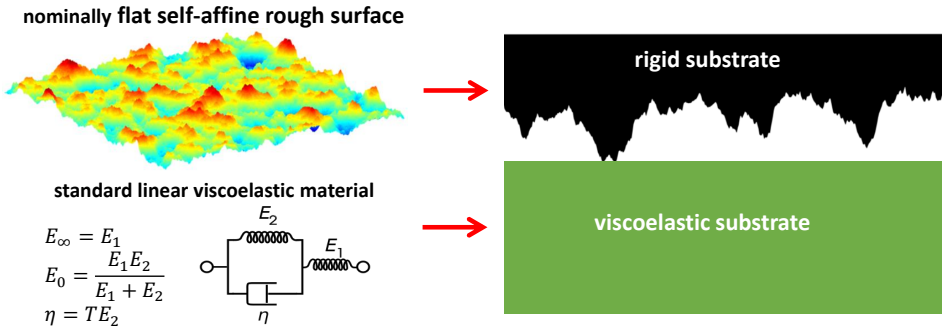

Figure 1: Top Left: a nominally flat randomly rough surface. Bottom left: a schematic representation of a standard linear viscoelastic material: a linear stiffness is in parallel with a damper and the both are in series with another spring. Right: in plane representation of the problem considered. A nominally flat rigid rough surface indents a flat viscoelastic substrate.

2. Persson's elastic solution for rough contact

In this section, the fundamental results of Persson's elastic contact mechanics for rough contact [47] are summarized, with particular emphasis on the dependence of the real contact area and mean separation on the average squeezing pressure.

Consider the contact between a flat elastic body with a nominally flat rigid substrate with self-affine random roughness and Gaussian height distribution. Persson [47] elastic solution gives the real contact area A as

$$\frac{A}{A_0} = \mathrm{erf}\left(\sqrt{\pi}\frac{p}{E^* h'_{rms}}\right) \tag{1}$$

where A_0 is the nominal contact area, $E^* = \frac{E}{1-\nu^2}$, with E the Young modulus and ν the Poisson ratio of the elastic body, h'_{rms} the root-mean-square slope of the rough surface, and p is the squeezing pressure. Notice that we have corrected the prefactor in Eq. (1) so that for small p one gets $\frac{A}{A_0} = \frac{2p}{E^* h'_{rms}}$, as found from numerical boundary element simulations [62, 63]. According to Yang & Persson [49], the relation between squeezing pressure and mean separation u is

$$p(u) = \beta q_0 h_{rms} E^* \exp(-u/u_0) \tag{2}$$

where $q_0 = \frac{2\pi}{\lambda_0}$ is the smallest wavenumber corresponding to the longest wavelength λ_0 in the rough surface representation, and h_{rms} is root-mean-square height roughness. For a general surface Power Spectral Density (PSD) $\Psi(q)$ and fractal dimension

$$u_0 = \sqrt{\pi}\gamma \int_{q_0}^{q_1} q^2 \Psi(q)\, \bar{w}(q)\, dq \tag{3}$$

$$\beta = \frac{\eta}{q_0 h_{rms}} \exp\left[-\frac{\int_{q_0}^{q_1} q^2 \Psi(q)\, \bar{w}(q) \log\left[\bar{w}(q)\right] dq}{\int_{q_0}^{q_1} q^2 \Psi(q)\, \bar{w}(q)\, dq} \right] \tag{4}$$

with

$$\bar{w}(q) = \left(\pi \int_{q_0}^{q} q'^3 \Psi(q')\, dq' \right)^{-1/2} \tag{5}$$

$$\eta = \exp\left[-\int_0^{\infty} \log x \left(6\frac{1-\gamma}{\gamma} P(x)\, P'(x) + \left[1 + 3\frac{1-\gamma}{\gamma} P^2(x) \right] (-2x) \right) \exp\left(-x^2\right) dx \right] \tag{6}$$

$$P(x) = \frac{2}{\sqrt{\pi}} \int_0^x \exp\left(-x'^2\right) dx' \tag{7}$$

where $P'(x) = dP(x)/dx$. From here on, we will restrict our attention to the typical case of a self-affine fractal surface with Hurst exponent close to $H = 0.8$. In the latter case, for small squeezing pressure ($u/u_0 \gtrsim 0.5$), one obtains $\beta \simeq 1$ and $u_0 \simeq 0.5 h_{rms}$ [64][65], which we shall use in the following derivations.

3. Viscoelastic solution

In this section, by using the correspondence principle of Lee and Radok [59], Persson's contact model for nominally flat rough contacts is extended to viscoelasticity. After deriving the theoretical model, it will be applied to both the cases of pressure and displacement step loading.

3.1. Theoretical background

To extend the elastic solution to the viscoelastic case, we use the correspondence principles of Lee and Radok [59], who showed how to deduce the viscoelastic solution of a contact problem from its elastic counterpart, provided that the contact area is monotonically increasing. Later, Ting [60]

extended Lee and Radok's approach, providing a method which permits to derive the viscoelastic solutions both when the contact area is increasing and when it is decreasing (see also Johnson [66] for the essential results). Lee and Radok's method gives the response at time t to a given stress $\sigma(t)$ (or strain $\varepsilon(t)$) history as it can be obtained superposing the response of small increment of stress (or strain). Hence, the strain response $\varepsilon(t)$ is found as

$$\varepsilon(t) = \sigma(0) C(t) + \int_0^t C(t-\tau) \frac{d\sigma(\tau)}{d\tau} d\tau \tag{8}$$

where $C(t)$ is the creep compliance function, i.e. the strain response to a unit stress increment $\sigma(t)$ in uniaxial stress conditions. Alternatively, the stress response $\sigma(t)$ is found as

$$\sigma(t) = \varepsilon(0) R(t) + \int_0^t R(t-\tau) \frac{d\varepsilon(\tau)}{d\tau} d\tau \tag{9}$$

where $R(t)$ is the relaxation function, i.e. the stress response to a unit of strain increment $\varepsilon(t)$ in uniaxial stress conditions. For a standard viscoelastic material, usually represented by the "three-element solid" (a spring in parallel with a dashpot and the pair in series with a second spring) we have

$$C(t) = \frac{1}{E_0^*} \left[1 - (1-k) \exp\left(-\frac{t}{T} \right) \right] \tag{10}$$

$$R(t) = E_0^* \left[1 + \left(\frac{1-k}{k} \right) \exp\left(-\frac{t}{kT} \right) \right] \tag{11}$$

where $k = E_0/E_\infty \ll 1$, being $E(\omega = 0) = E_0$ the relaxed modulus, $E(\omega = \infty) = E_\infty$ the instantaneous modulus and ω the excitation frequency. Notice that the creep compliance function and the relaxation function are physically meaningful for $t \geq 0$ and, as $k \ll 1$, the relaxation response to the strain increment is very much faster than the creep response to a stress increment. We assume Poisson's ratio be constant and independent on time, as usually is very close to 0.5 for these materials in any conditions.

Lee and Radok [59] showed that the solution of the viscoelastic contact problem is obtained by replacing the reciprocal of the elastic modulus $1/E^*$, in the elastic solution, by a convolution integral of the creep compliance $C(t)$ of the material. Hence, form Eq. (1) the elastic solution is written in the form

$$\operatorname{erf}^{-1} \frac{A}{A_0} = \sqrt{\pi} \frac{p}{E^* h'_{rms}} \tag{12}$$

and therefore the viscoelastic solution is

$$\mathrm{erf}^{-1}\frac{A\left(t\right)}{A_0}=\frac{\sqrt{\pi}}{h'_{rms}}\left(p\left(0\right)C\left(t\right)+\int_0^t C\left(t-\tau\right)\frac{dp\left(\tau\right)}{d\tau}d\tau\right) \tag{13}$$

which holds for any squeezing pressure history, as long as the contact area is increasing.

3.2. Step pressure loading

In particular, for a step loading $p\left(t\right)=p_0H\left(t\right)$, we have obviously

$$\frac{A\left(t\right)}{A_0}=\mathrm{erf}\left[\frac{\sqrt{\pi}}{h'_{rms}}C\left(t\right)p_0\right] \tag{14}$$

and for small p

$$\frac{A\left(t\right)}{A_0}=\frac{2p_0}{h'_{rms}}C\left(t\right) \tag{15}$$

which, in the limits of $t=0$ and $t=\infty$, gives Persson's elastic solution (1) with modulus E_∞ and E_0 respectively. For a standard viscoelastic material Eq. (10,14) give

$$\frac{A\left(t\right)}{A_0}=\mathrm{erf}\left(\sqrt{\pi}\frac{p_0}{E_0^*h'_{rms}}\left[1-\left(1-\frac{E_0}{E_\infty}\right)\exp\left(-\frac{t}{T}\right)\right]\right) \tag{16}$$

For the time evolution of the mean separation, one needs to substitute in the elastic pressure-separation relationship Eq. (2) the elastic modulus $1/E^*$ with the viscoelastic operator Eq. (8), which gives

$$\exp\left(-\frac{u\left(t\right)}{u_0}\right)=\frac{1}{\beta q_0h_{rms}}\left[p\left(0\right)C\left(t\right)+\int_0^t C\left(t-\tau\right)\frac{dp\left(\tau\right)}{d\tau}d\tau\right] \tag{17}$$

For pressure step loading $p\left(t\right)=p_0H\left(t\right)$, one obtains

$$\exp\left(-u\left(t\right)/u_0\right)=\frac{C\left(t\right)}{\beta q_0h_{rms}}p_0 \tag{18}$$

which for a standard viscoelastic material simplifies in

$$\frac{u\left(t\right)}{u_0}=-\log\left[\frac{p_0}{\beta q_0E_0^*h_{rms}}\left[1-\left(1-k\right)\exp\left(-\frac{t}{T}\right)\right]\right] \tag{19}$$

We introduce here the following dimensionless parameters

$$\widetilde{p}_0 = \frac{p_0}{E_0^* h'_{rms}}; \qquad \widetilde{A} = \frac{A}{A_0}; \qquad \widetilde{u} = \frac{u}{u_0}; \qquad \widetilde{t} = \frac{t}{T}; \qquad \chi = \frac{h'_{rms}}{\beta q_0 h_{rms}}; \tag{20}$$

In the following we will consider the most common case of a self-affine fractal surface with power law PSD and Hurst exponent $H = 0.8$, hence we have [67]

$$\chi(\zeta) = \sqrt{\frac{H}{1-H}} \frac{\zeta^{1-H}}{\beta} = \frac{2}{\beta} \zeta^{0.2} \tag{21}$$

where $\zeta = q_1/q_0$ is the surface "magnification", i.e. the ratio between the highest and the lowest wavenumber. With the above definitions Eq. (16) and Eq. (19) become respectively

$$\widetilde{A}(\widetilde{t}) = \operatorname{erf}\left(\sqrt{\pi}\widetilde{p}_0 \left[1 - (1-k)\exp\left(-\widetilde{t}\right)\right]\right) \tag{22}$$

$$\widetilde{u}\left(\widetilde{t}\right) = -\log\left[\widetilde{p}_0 \chi \left[1 - (1-k)\exp\left(-\widetilde{t}\right)\right]\right] \tag{23}$$

Figure 2a shows the dimensionless contact area as a function of time for $k = 0.01$, $\zeta = 10^3$ and varying $\widetilde{p}_0 = [0.01, 0.025, 0.05, 0.1]$. For a given squeezing pressure, due to the relaxation of the elastic modulus, the curves have a sigmoidal shape with the contact area that increases in time up to a plateau, corresponding to the elastic solution with Young modulus $E(\omega) = E_0$. For the same parameters Fig. 2b shows the time variation of the interfacial mean separation. Clearly, for $\widetilde{t} \ll 1$ the separation is large as the material is stiffer then in the relaxed state. As time passes, a creep process takes place that leads $\widetilde{u}\left(\widetilde{t}\right)$ to decrease up to the elastic solution with $E(\omega) = E_0$. Notice that the variation of contact area from $\widetilde{t} \ll 1$ to $\widetilde{t} \gg 1$ is much stronger than the variation of the mean separation as the creep compliance function $C(t)$ appears in Eq. (16) within the $\operatorname{erf}(x)$ function (which is almost linear for low $\widetilde{p}_0$), while in Eq. (19) $C(t)$ appears within the $\log(x)$ function.

3.3. Step displacement loading

Let us consider the case a remote displacement is imposed. We can apply the correspondence principles of Lee and Radok [59], as long as the contact area is growing. Substituting Eq. (2) into Eq. (1), we notice that the

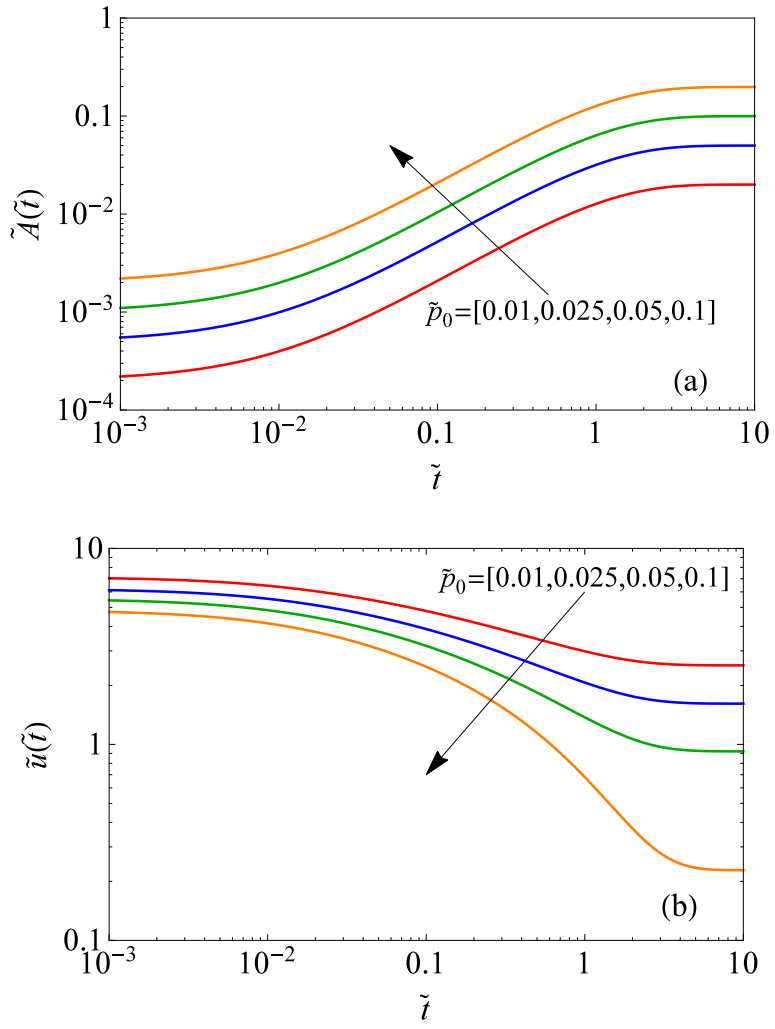

Figure 2: Dimensionless contact area (a) and mean separation (b) as a function of the dimensionless time for $k = 0.01$, $\zeta = 10^3$, $H = 0.8$ and varying $\widetilde{p}_0 = [0.01, 0.025, 0.05, 0.1]$, for step pressure loading. For a given squeezing pressure the contact area creeps in time and then reaches a maximum. For relatively low pressure, the ratio $\widetilde{A}(\widetilde{t} = 0^+)/\widetilde{A}(\widetilde{t} \to +\infty)$ is equal to the ratio of the moduli k. For a given squeezing pressure the mean separation diminishes in time as the elastic modulus relaxes.

area-separation relationship

$$\frac{A}{A_0} = \text{erf}\left(\sqrt{\pi}\frac{\beta q_0 h_{rms}}{h'_{rms}}\exp\left(-\frac{u}{u_0}\right)\right) \tag{24}$$

does not depend on the modulus and therefore, in the viscoelastic regime for imposed displacement, the real contact area is given by

$$\frac{A\left(t\right)}{A_0} = \mathrm{erf}\left(\sqrt{\pi}\frac{\beta q_0 h_{rms}}{h'_{rms}}\exp\left(-\frac{u\left(t\right)}{u_0}\right)\right) \tag{25}$$

However, the pressure as a function of time will relax, and we can replace the elastic modulus by the relaxation operator $R\left(t\right)$

$$p\left(t\right) = s\left(0\right)R\left(t\right) + \beta q_0 h_{rms}\int_0^t R\left(t-\tau\right)\frac{d}{d\tau}\exp\left(-\frac{1}{s\left(\tau\right)u_0}\right)d\tau \tag{26}$$

where we have defined $s(t) = u\left(t\right)^{-1}$. Hence, for a step displacement loading $s\left(t\right) = 0$ $\left(t < 0\right)$ and $s\left(t\right) = 1/u_1$ $\left(t > 0\right)$, we have $\exp\left(-1/s\left(\tau\right)u_0\right) = 0$ $\left(t < 0\right)$ and $\exp\left(-1/s\left(\tau\right)u_0\right) = \exp\left(-u_1/u_0\right)$ $\left(t > 0\right)$, which we can write as $\exp\left(-1/s\left(\tau\right)u_0\right) = H\left(\tau\right)\exp\left(-u_1/u_0\right)$, hence

$$\frac{d}{d\tau}\left(H\left(\tau\right)\exp\left(-\frac{u_1}{u_0}\right)\right) = \exp\left(-\frac{u_1}{u_0}\right)\delta\left(\tau\right) \tag{27}$$

where $\delta\left(\tau\right)$ is the Dirac delta function. Substituting Eq. (27) into Eq. (26) one gets

$$p\left(t\right) = \beta q_0 h_{rms} R\left(t\right)\exp\left(-\frac{u_1}{u_0}\right) \tag{28}$$

which, using Eq. (11) for a standard viscoelastic material, gives

$$p\left(t\right) = \beta q_0 h_{rms} E_0^*\left[1 + \frac{\left(1-k\right)}{k}\exp\left(-\frac{t}{kT}\right)\right]\exp\left(-\frac{u_1}{u_0}\right) \tag{29}$$

or, in dimensionless form

$$\widetilde{p}\left(\widetilde{t}\right) = \frac{1}{\chi}\left[1 + \frac{\left(1-k\right)}{k}\exp\left(-\frac{\widetilde{t}}{k}\right)\right]\exp\left(-\widetilde{u}_1\right) \tag{30}$$

Figure 3 shows, for the same parameters used in Fig. 2 but $\widetilde{u}_1 = [1, 2, 3, 4]$, the relaxation of the squeezing pressure as a function of time, as one would expect from the relation of the Young's modulus from E_∞ to E_0. Notice that for imposed displacement $\frac{\widetilde{p}\left(\widetilde{t}\to+\infty\right)}{\widetilde{p}\left(\widetilde{t}=0^+\right)} = \frac{E_0}{E_\infty}$.

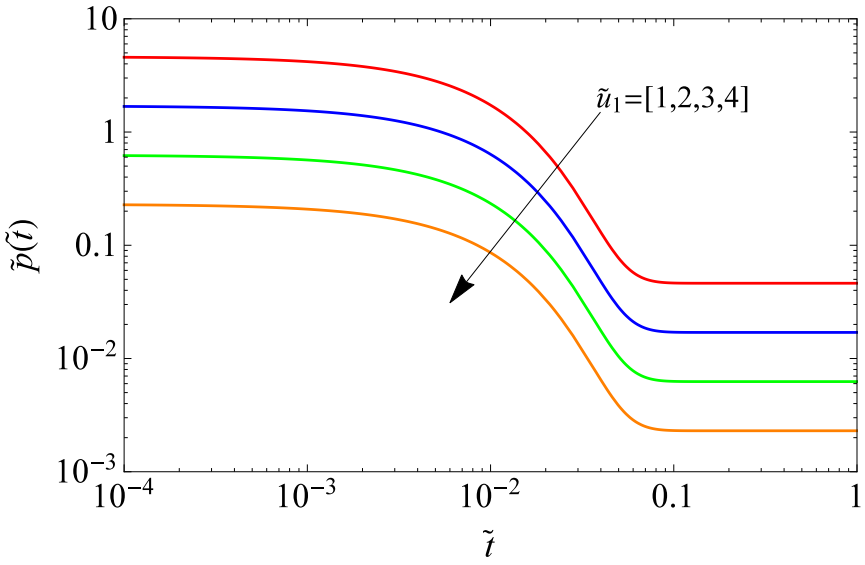

Figure 3: Average squeezing pressure versus time for $k = 0.01$, $\zeta = 10^3$, $H = 0.8$ and varying $\widetilde{u}_1 = [1, 2, 3, 4]$ for step displacement loading. For a given displacement the mean pressure $\widetilde{p}$ decreases with time as the elastic modulus of the material relaxes. The ratio $\widetilde{p}\left(\widetilde{t} \to +\infty\right)/\widetilde{p}\left(\widetilde{t} = 0^+\right)$ is equal to the ratio of the moduli of the material k.

4. Oscillatory loading

In this section, the case of harmonic pressure loading is considered. First, the theoretical model is derived, then some macroscopic quantities of general interest in soft viscoelastic contacts are determined such as the real contact area, the mean separation and the dissipated energy per loading cycle.

4.1. Theoretical model

It is interesting to observe the behavior of the contact upon unloading, or indeed oscillatory loading, as this would be important for determining the energy dissipated in a loading cycle, a quantity of general interest particularly for determining the damping properties of soft interfaces subjected to cyclic loads. We shall restrict ourselves to the first loading. Let us assume the applied pressure has the harmonic form

$$p\left(t\right) = p_0\left[\alpha + \sin\left(t/T_{load} - \gamma\right)\right] \tag{31}$$

with $\gamma = \arcsin(\alpha)$ and $-1 \leq \alpha \leq 1$ so that the condition $p(t=0) = 0$ is always satisfied. As the contact problem we are addressing is adhesiveless, we will consider only the time interval during which the load is compressive, hence the analysis will be restricted to the interval $t/T_{load} \in [0, \pi + 2\gamma]$.

Ting [60] has provided a general solution method for obtaining the viscoelastic solution during unloading, which is here used. As in the previous section, we can use Lee and Radok's [59] method up to the time $t = t_m$ when the contact area $A(t)/A_0$ reaches its maximum (t_m depends on the material). For $t > t_m$ we need to use the relaxation operator. Ting [60] showed that when $A(t)$ is decreasing, the contact pressure at time t depends only upon the contact stress history up to time t_1, where $t_1 < t_m$ and

$$A(t_1) = A(t) \tag{32}$$

therefore the equations valid when the contact area is growing can still be used. Hence, using Lee and Radok method, from Eq. (13) we write the viscoelastic convolution

$$\operatorname{erf}^{-1} \frac{A(t)}{A_0} = \frac{\sqrt{\pi}}{h'_{rms}} \left[\frac{p_0}{T_{load}} \int_0^t C(t-\tau) \cos\left(\frac{\tau}{T_{load}} - \gamma \right) d\tau \right] \tag{33}$$

from which the time $t = t_m$ where the contact area reaches its maximum can be determined. To find the time t_1 we use the standard method of Lee and Radok to transform the elastic load-area relation (Eq. (1)) to the viscoelastic case during growing contact area (starting from $A(0) = 0$)

$$\begin{aligned} p(t) &= \frac{h'_{rms}}{\sqrt{\pi}} \int_0^{t_1} R(t-t') \frac{d}{dt'} \left(\operatorname{erf}^{-1} \frac{A(t')}{A_0} \right) dt' = \\ &= \frac{p_0}{T_{load}} \int_0^{t_1} R(t-t') \left[C(0) \cos\left(\frac{t'}{T_{load}} - \gamma \right) + \int_0^{t'} C'(t'-\tau) \cos\left(\frac{\tau}{T_{load}} - \gamma \right) d\tau \right] dt' \end{aligned} \tag{34}$$

where we used Eq. (33), $C'(t'-\tau) = \frac{d}{dt'} C(t'-\tau)$ and the upper limit of integration is $t = t_1$. Equating this result to the form of the pressure loading (Eq. (31)), we derive an equation for t_1 as a function of t. For a standard viscoelastic material it leads to

$$\sin\left(\frac{t}{T_{load}}-\gamma\right)=\left\{\sin\left(\frac{t_1}{T_{load}}-\gamma\right)-\frac{(1-k)\left(1-\exp\left(-\frac{t-t_1}{kT}\right)\right)}{1+\left(\frac{T_{load}}{T}\right)^2}*\right.$$
$$\left.*\left[\sin\left(\frac{t_1}{T_{load}}-\gamma\right)+\frac{T_{load}}{T}\cos\left(\frac{t_1}{T_{load}}-\gamma\right)-\left(\frac{T_{load}}{T}\cos\gamma-\sin\gamma\right)\exp\left(\frac{-t_1}{T}\right)\right]\right\} \tag{35}$$

which for the case $\alpha=0$ reduces to Eq. (9) in Ref. [61][1].

After the contact area has been found, to find the mean separation, consider that in the viscoelastic regime, as long as the contact area is growing, the elastic relation holds, which is

$$\frac{u\left(t\right)}{u_0}=-\log\left[\frac{h'_{rms}}{\sqrt{\pi}\beta q_0 h_{rms}}\operatorname{erf}^{-1}\frac{A\left(t\right)}{A_0}\right] \tag{36}$$

or in dimensionless form

$$\widetilde{u}\left(t\right)=-\log\left[\frac{\widetilde{p}_0\chi E_0^*}{T_{load}}\int_0^t C\left(t-\tau\right)\cos\left(\frac{\tau}{T_{load}}-\gamma\right)d\tau\right] \tag{37}$$

For the unloading, Greenwood [61] has suggested that a simpler solution than Ting's is obtained defining

$$G\left(t,\tau\right)=1-C\left(0\right)R\left(t\right)+\int_{x=\tau}^t R\left(x\right)\frac{d}{dx}C\left(t-x\right)dx \tag{38}$$

giving the response at time t to a unit displacement applied at time $t=0$ and removed at time $t=\tau$ so as to leave the surface stress-free at the time $t>\tau$. Notice that this function is a material property, so it is the same found by Greenwood when studying the axisymmetric Hertzian contact [61]. In particular, for a standard viscoelastic material Greenwood [61] gives

$$G\left(t,\tau\right)=(1-k)\left[1-\exp\left(-\frac{\tau}{kT}\right)\right]\exp\left(-\frac{(t-\tau)}{T}\right) \tag{39}$$

Therefore, summing up the response of small displacement increments we find the displacement at time t to be

$$u\left(t\right)=u\left(t_1\right)+\int_{x=t_1}^{t_m}\frac{\partial u\left(x\right)}{\partial x}G\left(t-x,\tau\left(x\right)-x\right)dx \tag{40}$$

[1]We have corrected a typo in Ref. [61].

where t_1 is the time at which the current area $A(t)$ was first reached (when the area was increasing), while $\tau(x)$ is the time when that contact area $A(x)$ was removed. Solving numerically Eq. (40) poses some challenges as $\lim_{t\to 0} u(t) = +\infty$. To overcome this difficulty, we used $s(t) = u(t)^{-1}$ so that, following the procedure as above, Eq. (40) can be written as

$$u(t) = \left[s(t_1) + \int_{x=t_1}^{t_m} \frac{\partial s(x)}{\partial x} G(t - x, \tau(x) - x)\, dx \right]^{-1} \tag{41}$$

and for $t > (\pi + 2\gamma) T_{load}$ when the surface is left stress free

$$u(t) = \left[\int_{x=0}^{t_m} \frac{\partial s(x)}{\partial x} G(t - x, \tau(x) - x)\, dx \right]^{-1} \tag{42}$$

which is easier to solve numerically as $\lim_{t\to 0} s(t) = 0$, which guarantees a smooth transition from Eq. (41) to Eq. (42).

4.2. Time evolution of contact area and mean separation

Figure 4 shows the dimensionless (a) contact area and (b) mean separation for $k = 0.1$, $\zeta = 10^3$, $\widetilde{p}_0 = 0.05$, $\alpha = 0$ and varying $T_{load}/T = [0.01, 0.05, 0.1, 0.2, 0.5, 1, 2, 100]$, where we have indicated in blue the time interval $t \in [0, t_m]$, while the contact area is growing, and in red the interval when the contact area is decreasing. High loading periods T_{load} lead to larger contact area and low mean separation as the material is more compliant. Fast loading (low T_{load}) leads instead to a small contact area and high mean separation as the material is stiffer. We notice that for both high and low T_{load}/T ratio the solution is elastic (indeed, the curve are symmetric with respect to $t/T_{load} = \pi/2$) and there would not be (in the limit) any dissipated energy. In the intermediate cases, both the $\widetilde{A}(t)$ and $\widetilde{u}(t)$ curves are skewed, which is a sign that viscoelastic dissipation is taking place. Also, for the case we have considered with $\alpha = 0$, the load is removed at $t = \pi T_{load}$, which appears in the $\widetilde{u}(t)$ curves, particularly for intermediate values of T_{load}/T where it can be distinguished clearly the viscoelastic substrate relaxation following the removal of the normal load.

Figure 5ab looks at the effect of a different mean normal load, through the variation of the coefficient $\alpha = [-0.8, -0.4, 0, 0.4, 0.8, 1]$. Panel (a) shows the contact area while panel (b) shows the mean separation as a function of time for the same parameters as in Fig. 4 and $T_{load}/T = 0.1$. Increasing α increases the mean normal load in a loading cycle, as $p(t)$ is compressive

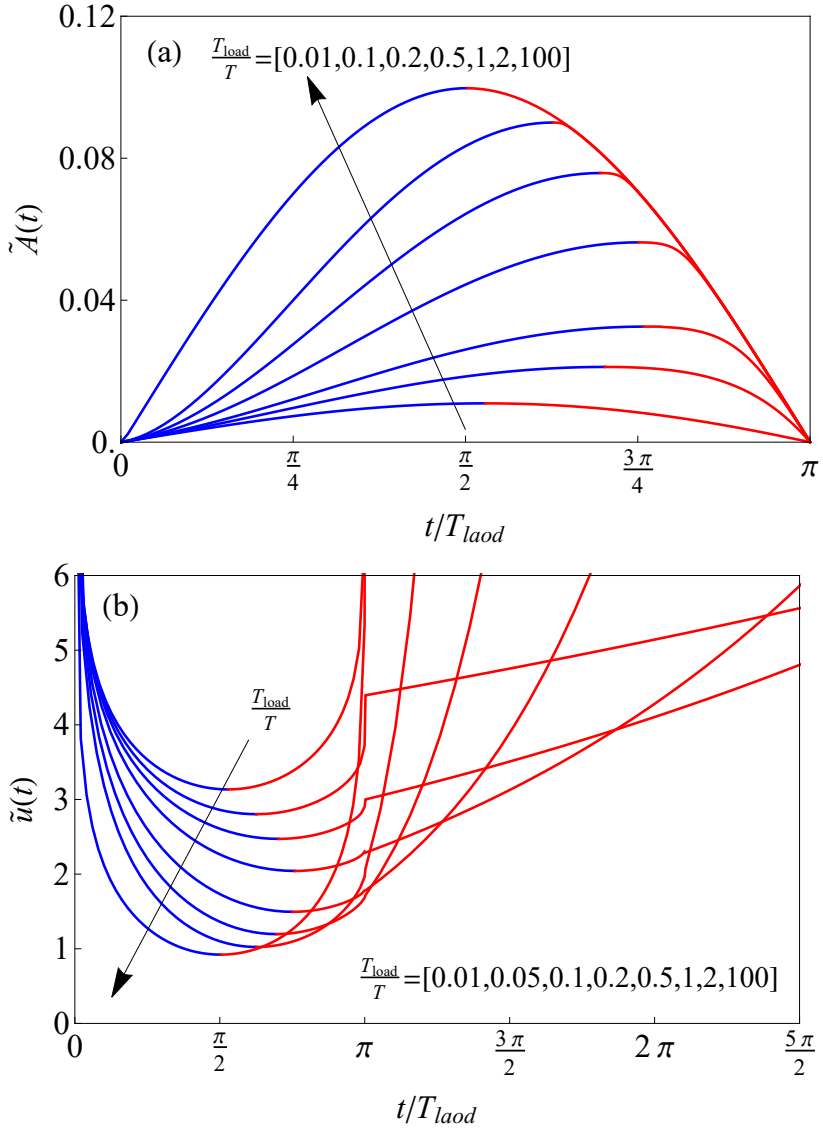

Figure 4: (a) Dimensionless contact area and (b) mean separation as a function of the ratio t/T_{load} for $k = 0.1$, $\zeta = 10^3$, $H = 0.8$, $\widetilde{p}_0 = 0.05$, $\alpha = 0$ and varying $T_{load}/T = [0.01, 0.05, 0.1, 0.2, 0.5, 1, 2, 100]$. The blue and red curves refer respectively to the time intervals when the contact area is increasing or decreasing. For $t/T_{load} \geq \pi$ the squeezing pressure vanishes and so does the contact area, while the mean separation relaxes.

in the time interval $t \in [0, \pi + 2\arcsin(\alpha)]$. Consequently, panel (a) shows that the contact area gets larger and the contact time interval increases. Furthermore, the longer the contact interval (large α), the smaller the mean separation gets. These results suggest that α will play a crucial role in determining the amount of energy that gets dissipated when a viscoelastic contact is loaded and unloaded, which we shall investigate in the next section.

4.3. Viscoelastic dissipation

A crucial quantity to be determined when interfaces are loaded and unloaded is the energy that gets dissipated in an indentation cycle. Figure 6 shows few exemplary loading cycles for $k = 0.1$, $\zeta = 10^3$, $\widetilde{p}_0 = 0.05$, $\alpha = 0$ and for varying $T_{load}/T = [10^{-3}, 10^{-1}, 10^0, 10^3]$. It is shown that both very high and very low T_{load} leads to an elastic response of the material where the loading and the unloading curves coincide. For $T_{load}/T = [10^{-1}, 10^0]$, instead, viscoelastic effects are clearly at play with differing loading path at loading and unloading that give viscoelastic bulk dissipation (for the $T_{load}/T = 10^{-1}$, we have shaded the area enclosed in the loading cycle that is proportional the dissipated energy). In Fig. 6 the red curves correspond to the interval with growing contact area, while the blue curves correspond to those with decreasing contact area, from which one sees that the area time evolution lags back with respect to the load.

The external energy spent per unit area deforming the viscoelastic material in dimensionless form reads

$$\widetilde{U} = \frac{U}{p_0 u_0} = \int_0^{(\pi+2\gamma)T_{load}} \left(\alpha + \sin\left(\frac{t}{T_{load}} - \gamma\right)\right) \frac{d\widetilde{u}}{dt} dt \tag{43}$$

Figure 7a shows the dissipated energy $|\widetilde{U}|$ as a function of T_{load}/T for $k = [10^{-3}, 10^{-2}, 10^{-1}]$, $\widetilde{p}_0 = 0.05$, $\zeta = 10^3$ and $\alpha = 0$. We recognize that for high and low T_{load}/T ratio $|\widetilde{U}|$ vanishes as the contact behaves as elastic, while in the intermediate region and close to $T_{load}/T \simeq 1$ the maximum dissipation is obtained. The dissipation decreases as E_0 approaches E_∞ (increasing k), which also slightly influences the maximum location. The dissipated energy further increases by increasing α as it is shown in panel (b) where we fixed $E_0/E_\infty = 10^{-1}$ and varied the mean normal load by varying the parameter $\alpha = [-0.5, 0, 0.5, 1]$. We conclude that generally the best damping performance will be obtained for vanishing E_0/E_∞ (so-called "liquid" material)

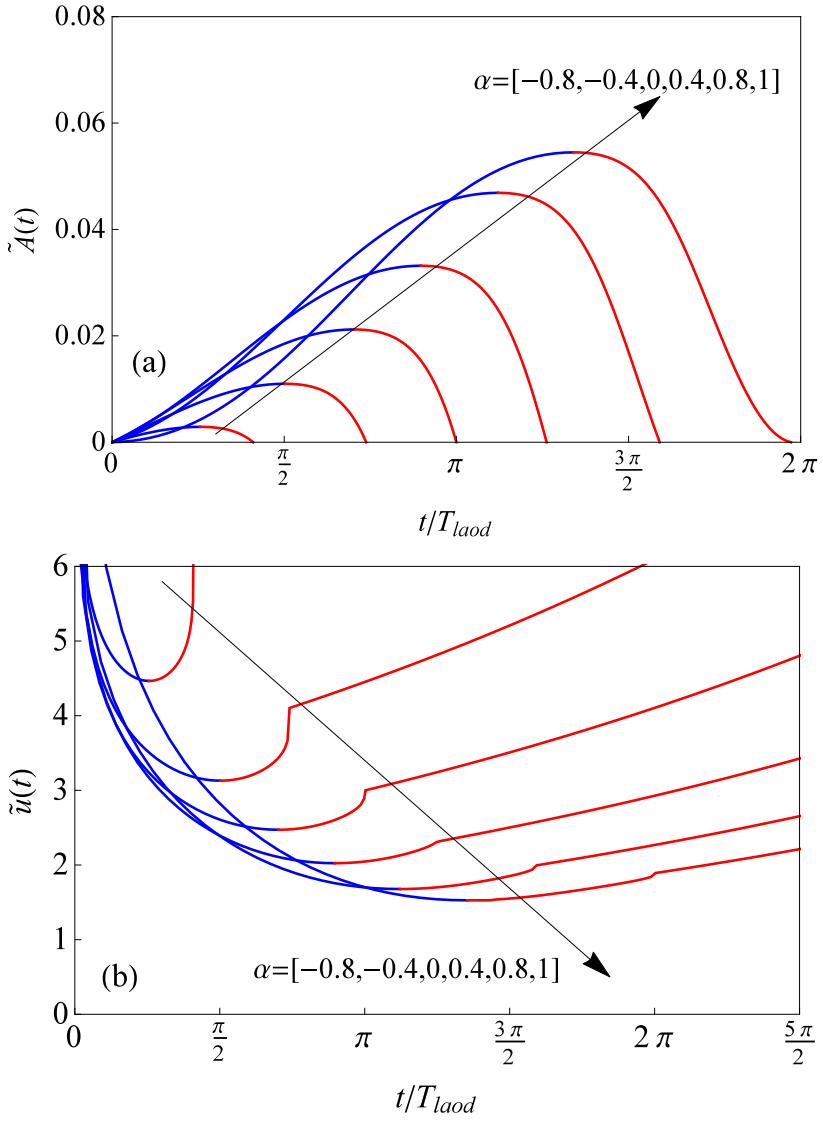

Figure 5: (a) Dimensionless contact area and (b) mean separation as a function of the ratio t/T_{load} for $k = 0.1$, $\zeta = 10^3$, $H = 0.8$, $\widetilde{p}_0 = 0.05$, $T_{load}/T = 0.1$ and varying $\alpha = [-0.8, -0.4, 0, 0.4, 0.8, 1]$. Blue and red curves refer respectively to the time intervals when the contact area is increasing or decreasing. By increasing α, increases the maximum squeezing pressure, hence one gets a larger contact area and a lower mean separation.

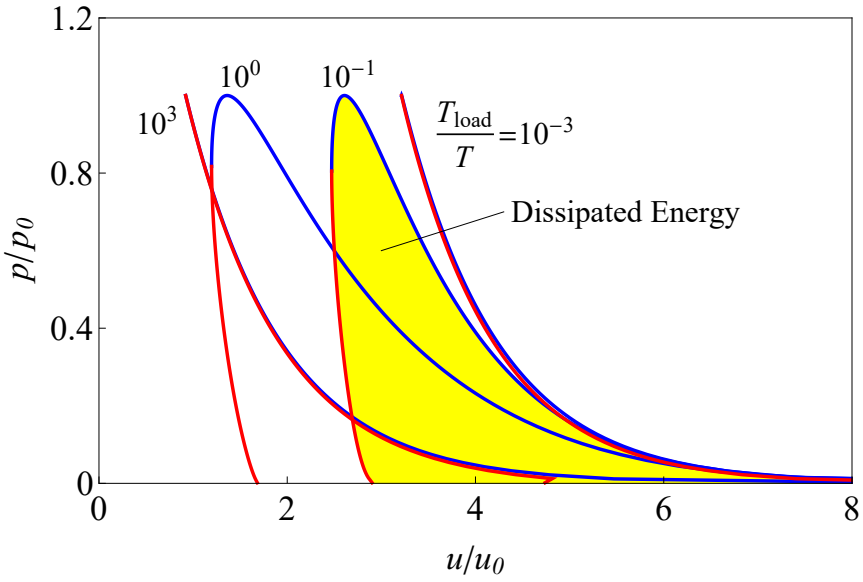

Figure 6: An example of four loading cycles obtained with $k = 0.1$, $\zeta = 10^3$, $H = 0.8$, $\widetilde{p}_0 = 0.05$, $\alpha = 0$, $T_{load}/T = \left[10^{-3}, 10^{-1}, 10^0, 10^3\right]$. Blue and red curves refer respectively to the time intervals when the contact area is increasing or decreasing. The area enclosed in the hysteresis loop is proportional to the dissipated energy in the first loading cycle. For the case $T_{load}/T = 10^{-1}$ it is shaded in yellow. One sees that both cases of high and low loading period lead to a vanishing dissipation.

for high mean load and in the range $10^{-2} \lesssim T_{load}/T \lesssim 10^0$.

5. Conclusions

In this manuscript, the Persson elastic theories for the contact of nominally flat bodies with randomly rough surfaces have been extended to the case of viscoelasticity by using the correspondence principle of Lee and Radok [59] and the following extensions by Ting [60] and Greenwood [61]. The case of a rigid rough surface that indents a standard linear viscoelastic substrate has been considered in detail, although the equations are written in general form and the same procedure can be applied to any linear viscoelastic material once the creep compliance and the relaxation functions are known.

We have considered both the cases of pressure and displacement step loading. It has been shown that for step pressure loading the real contact area A creeps in time. For low squeezing pressure, the ratio $A(t = 0^+)/A(t \rightarrow$

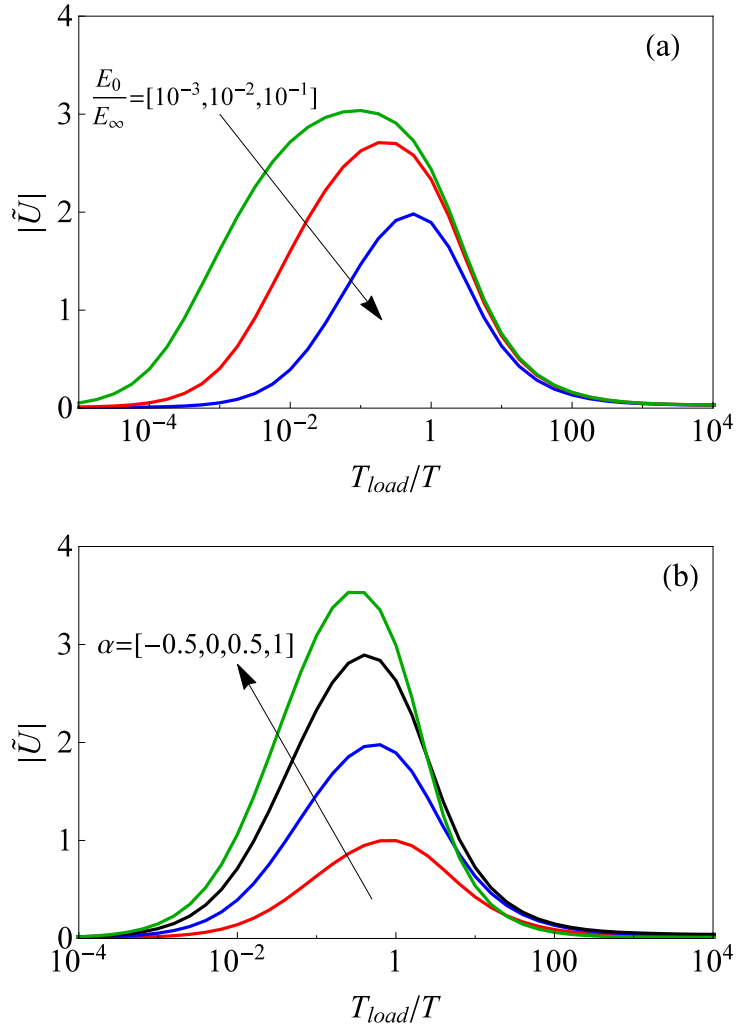

Figure 7: Dimensionless dissipated energy versus T_{load}/T for (a) $E_0/E_\infty = [10^{-3}, 10^{-2}, 10^{-1}]$, and $\alpha = 0$ and (b) $E_0/E_\infty = 10^{-1}$, and $\alpha = [-0.5, 0, 0.5, 1]$. The dissipated energy in the first loading cycle increases by increasing α and by decreasing the ratio between the moduli k. In both panels $\zeta = 10^3$, $H = 0.8$, and $\widetilde{p}_0 = 0.05$.

$+\infty$) is equal to the ratio of the moduli $k = E_0/E_\infty$. For step displacement loading the average squeezing pressure p relaxes (diminishes) in time with the ratio $p(t \to +\infty)/p(t = 0^+) = k$.

Exploiting Ting's extension of Lee and Radok's method, we have considered a full cycle of harmonic loading and unloading, with differing squeezing pressure mean value. This was particularly interesting to determine the viscoelastic bulk dissipation, i.e the energy that gets dissipated per unit nominal area per loading cycle. It has been shown that the maximum dissipation is obtained when the loading period is close to the relaxation time of the material and is increased by increasing the mean normal pressure and decreasing the ratio between the relaxed and instantaneous moduli of the viscoelastic material E_0/E_∞.

Acknowledgements

AP and MC acknowledge support from the Italian Ministry of Education, University and Research (MIUR) under the program "Departments of Excellence" (L.232/2016). A.P. acknowledges support from "PON Ricerca e Innovazione 2014-2020-Azione I.2" - D.D. n. 407, 27/02/2018, bando AIM (Grant No. AIM1895471).

References

[1] Shepherd, R. F., Ilievski, F., Choi, W., Morin, S. A., Stokes, A. A., Mazzeo, A. D., ... & Whitesides, G. M. (2011). Multigait soft robot. Proceedings of the national academy of sciences, 108(51), 20400-20403.

[2] Shintake, J., Cacucciolo, V., Floreano, D., & Shea, H. (2018). Soft robotic grippers. Advanced Materials, 30(29), 1707035.

[3] Nakra, B. C. (1998). Vibration control in machines and structures using viscoelastic damping. Journal of sound and vibration, 211(3), 449-466.

[4] Rao, M. D. (2003). Recent applications of viscoelastic damping for noise control in automobiles and commercial airplanes. Journal of Sound and Vibration, 262(3), 457-474.

[5] Jones, D. I. (2001). Handbook of viscoelastic vibration damping. John Wiley & Sons.

[6] Zhou, X. Q., Yu, D. Y., Shao, X. Y., Zhang, S. Q., & Wang, S. (2016). Research and applications of viscoelastic vibration damping materials: A review. Composite Structures, 136, 460-480.

[7] Krishna, V. V., Saravanamurugan, S., Kishore, P. S., Yedhu, K. J., Iswar, G. K., & Shanmughasundaram, A. (2021, February). Vibration control in boring process using a constrained viscoelastic layer damper. In IOP Conference Series: Materials Science and Engineering (Vol. 1059, No. 1, p. 012031). IOP Publishing.

[8] Papangelo, A. (2021). On the effect of shear loading rate on contact area shrinking in adhesive soft contacts. Tribology letters, 69(2), 1-9.

[9] Persson, B. N. J. (1995). Theory of friction: Stress domains, relaxation, and creep. Physical Review B, 51(19), 13568.

[10] Beeler, N. M., Tullis, T. E., & Weeks, J. D. (1994). The roles of time and displacement in the evolution effect in rock friction. Geophysical Research Letters, 21(18), 1987-1990.

[11] Papangelo, A. (2021). On the Effect of a Rate-Dependent Work of Adhesion in the Detachment of a Dimpled Surface. Applied Sciences, 11(7), 3107.

[12] Scholz, C. H. (1998). Earthquakes and friction laws. Nature, 391(6662), 37-42.

[13] Buezas, F. S., & Fochesatto, N. S. (2018). Power dissipation of a viscoelastic rolling wheel in finite deformations. International Journal of Mechanical Sciences, 138, 502-514.

[14] Creton, C., & Leibler, L. (1996). How does tack depend on time of contact and contact pressure?. Journal of Polymer Science Part B: Polymer Physics, 34(3), 545-554

[15] Peng, B., Li, Q., Feng, X. Q., & Gao, H. (2021). Effect of shear stress on adhesive contact with a generalized Maugis-Dugdale cohesive zone model. Journal of the Mechanics and Physics of Solids, 148, 104275.

[16] Das, D., Chasiotis, I.: Sliding of Adhesive Nanoscale Polymer Contacts. Journal of the Mechanics and Physics of Solids, 103931, (2020). DOI: 10.1016/j.jmps.2020.103931

[17] Ciavarella, M., & Papangelo, A. (2020). On the degree of irreversibility of friction in sheared soft adhesive contacts. Tribology Letters, 68(3), 1-9.

[18] Sahli, R., Pallares, G., Ducottet, C., Ali, I. B., Al Akhrass, S., Guibert, M., & Scheibert, J. (2018). Evolution of real contact area under shear and the value of static friction of soft materials. Proceedings of the National Academy of Sciences, 115(3), 471-476.

[19] McMeeking, R. M., Ciavarella, M., Cricrì, G., & Kim, K. S. (2020). The interaction of frictional slip and adhesion for a stiff sphere on a compliant substrate. Journal of Applied Mechanics, 87(3), 031016.

[20] Wang, J., Tiwari, A., Sivebaek, I. M., & Persson, B. N. J. (2020). Sphere and cylinder contact mechanics during slip. Journal of the Mechanics and Physics of Solids, 143, 104094.

[21] Genovese, A., Farroni, F., Papangelo, A., & Ciavarella, M. (2019). A discussion on present theories of rubber friction, with particular reference to different possible choices of arbitrary roughness cutoff parameters. Lubricants, 7(10), 85.

[22] Tolpekina, T. V., & Persson, B. N. J. (2019). Adhesion and friction for three tire tread compounds. Lubricants, 7(3), 20.

[23] Le Gal, A., Yang, X., & Klüppel, M. (2005). Evaluation of sliding friction and contact mechanics of elastomers based on dynamic-mechanical analysis. The Journal of chemical physics, 123(1), 014704.

[24] Le Gal, A., & Klüppel, M. (2007). Investigation and modelling of rubber stationary friction on rough surfaces. Journal of Physics: Condensed Matter, 20(1), 015007.

[25] Lang, A., & Klüppel, M. (2017). Influences of temperature and load on the dry friction behaviour of tire tread compounds in contact with rough granite. Wear, 380, 15-25.

[26] Persson, B. N. J., & Volokitin, A. I. (2006). Rubber friction on smooth surfaces. The European Physical Journal E, 21(1), 69-80.

[27] Lengiewicz, J., de Souza, M., Lahmar, M. A., Courbon, C., Dalmas, D., Stupkiewicz, S., & Scheibert, J. (2020). Finite deformations govern the anisotropic shear-induced area reduction of soft elastic contacts. Journal of the Mechanics and Physics of Solids, 143, 104056.

[28] Chateauminois, A., & Fretigny, C. (2008). Local friction at a sliding interface between an elastomer and a rigid spherical probe. The European Physical Journal E, 27(2), 221-227.

[29] Mergel, J. C., Sahli, R., Scheibert, J., & Sauer, R. A. (2019). Continuum contact models for coupled adhesion and friction. The Journal of Adhesion. 95(12), 1101-1133

[30] Hwu, C. (2020). Time-stepping method for frictional contact of anisotropic viscoelastic solids. International Journal of Mechanical Sciences, 184, 105836.

[31] Hwu, C. (2020). Indentation by multiple rigid punches on two-dimensional anisotropic elastic or viscoelastic solids. International Journal of Mechanical Sciences, 178, 105595.

[32] Putignano, C. (2021). Oscillating viscoelastic periodic contacts: A numerical approach. International Journal of Mechanical Sciences, 208, 106663.

[33] Feng, C., Zhang, D., Chen, K., & Guo, Y. (2018). Study on viscoelastic friction and wear between friction linings and wire rope. International Journal of Mechanical Sciences, 142, 140-152.

[34] Bowden, F. P., Bowden, F. P., & Tabor, D. (2001). The friction and lubrication of solids (Vol. 1). Oxford university press.

[35] Shooter, K. V., & Tabor, D. (1952). The frictional properties of plastics. Proceedings of the Physical Society. Section B, 65(9), 661.

[36] Greenwood, J. A., & Williamson, J. P. (1966). Contact of nominally flat surfaces. Proceedings of the royal society of London. Series A. Mathematical and physical sciences, 295(1442), 300-319.

[37] Fineberg, J., & Bouchbinder, E. (2015). Recent developments in dynamic fracture: some perspectives. International Journal of Fracture, 196(1-2), 33-57.

[38] Rubinstein, S. M., Cohen, G., & Fineberg, J. (2004). Detachment fronts and the onset of dynamic friction. Nature, 430(7003), 1005-1009.

[39] Svetlizky, I., Kammer, D. S., Bayart, E., Cohen, G., & Fineberg, J. (2017). Brittle fracture theory predicts the equation of motion of frictional rupture fronts. Physical review letters, 118(12), 125501.

[40] Berman, N., Cohen, G., & Fineberg, J. (2020). Dynamics and properties of the cohesive zone in rapid fracture and friction. Physical Review Letters, 125(12), 125503.

[41] Afferrante, L., Bottiglione, F., Putignano, C., Persson, B. N. J., & Carbone, G. J. T. L. (2018). Elastic contact mechanics of randomly rough surfaces: an assessment of advanced asperity models and Persson's theory. Tribology Letters, 66(2), 1-13.

[42] Bhushan, B. (1998). Contact mechanics of rough surfaces in tribology: multiple asperity contact. Tribology letters, 4(1), 1-35.

[43] Carbone, G., & Bottiglione, F. (2011). Contact mechanics of rough surfaces: a comparison between theories. Meccanica, 46(3), 557-565.

[44] Campaná, C., & Müser, M. H. (2007). Contact mechanics of real vs. randomly rough surfaces: A Green's function molecular dynamics study. EPL (Europhysics Letters), 77(3), 38005.

[45] Pastewka L, Robbins MO. (2014) Contact between rough surfaces and a criterion for macroscopic adhesion. Proc. Natl Acad. Sci. USA 111, 3298–3303.

[46] Bush, A. W., Gibson, R. D., & Thomas, T. R. (1975). The elastic contact of a rough surface. Wear, 35(1), 87-111.

[47] Persson, BNJ. "Theory of rubber friction and contact mechanics." The Journal of Chemical Physics 115, no. 8 (2001): 3840-3861.

[48] Persson, B. N. J. (2007). Relation between interfacial separation and load: a general theory of contact mechanics. Physical review letters, 99(12), 125502.

[49] Yang, C., & Persson, B. N. J. (2008). Contact mechanics: contact area and interfacial separation from small contact to full contact. Journal of Physics: Condensed Matter, 20(21), 215214.

[50] Hyun, S., Pei, L., Molinari, J. F., & Robbins, M. O. (2004). Finite-element analysis of contact between elastic self-affine surfaces. Physical Review E, 70(2), 026117.

[51] Joe, J., Scaraggi, M., & Barber, J. R. (2017). Effect of fine-scale roughness on the tractions between contacting bodies. Tribology International, 111, 52-56.

[52] Pei, L., Hyun, S., Molinari, J. F., & Robbins, M. O. (2005). Finite element modeling of elasto-plastic contact between rough surfaces. Journal of the Mechanics and Physics of Solids, 53(11), 2385-2409.

[53] Prodanov, N., Dapp, W. B., & Müser, M. H. (2014). On the contact area and mean gap of rough, elastic contacts: Dimensional analysis, numerical corrections, and reference data. Tribology Letters, 53(2), 433-448.

[54] Rey, V., Anciaux, G., & Molinari, J. F. (2017). Normal adhesive contact on rough surfaces: efficient algorithm for FFT-based BEM resolution. Computational Mechanics, 60(1), 69-81.

[55] Sainsot, P., Lubracht A.A., (2011). Efficient solution of the dry contact of rough surfaces: a comparison of fast Fourier transform and multigrid methods. Proceedings of the Institution of Mechanical Engineers, Part J: Journal of Engineering Tribology, 225(6), 441-448.

[56] Vollebregt, E., (2014). A new solver for the elastic normal contract problem using conjugate gradients, deflation, and an FFT-based preconditioner. Tribology International, 125, 169-199.

[57] Yang, C., Tartaglino, U., & Persson, B. N. J. (2006). A multiscale molecular dynamics approach to contact mechanics. The European Physical Journal E, 19(1), 47-58.

[58] Yastrebov, V. A., Durand, J., Proudhon, H., & Cailletaud, G. (2011). Rough surface contact analysis by means of the finite element method

and of a new reduced model. Comptes Rendus Mécanique, 339(7-8), 473-490.

[59] Lee, E. H., and Radok JRM. "The contact problem for viscoelastic bodies." (1960): 438-444.

[60] Ting, T. C. T. (1966). The contact stresses between a rigid indenter and a viscoelastic half-space.

[61] Greenwood, J. A. (2010). Contact between an axisymmetric indenter and a viscoelastic half-space. International Journal of Mechanical Sciences, 52(6), 829-835.

[62] Putignano, C., Afferrante, L., Carbone, G., & Demelio, G. (2012). The influence of the statistical properties of self-affine surfaces in elastic contacts: A numerical investigation. Journal of the Mechanics and Physics of Solids, 60(5), 973-982.

[63] M*ü*ser, M. H., Dapp, W. B., Bugnicourt, R., Sainsot, P., Lesaffre, N., Lubrecht, T. A., ... & Greenwood, J. A. (2017). Meeting the contact-mechanics challenge. Tribology Letters, 65(4), 1-18.

[64] Pei, L., Hyun, S., Molinari, J. F., & Robbins, M. O. (2005). Finite element modeling of elasto-plastic contact between rough surfaces. Journal of the Mechanics and Physics of Solids, 53(11), 2385-2409.

[65] Papangelo, A., Hoffmann, N., & Ciavarella, M. (2017). Load-separation curves for the contact of self-affine rough surfaces. Scientific reports, 7(1), 1-7.

[66] Johnson, K. L., (1987). Contact mechanics. Cambridge university press.

[67] Violano, G., Afferrante, L., Papangelo, A., & Ciavarella, M. (2019). On stickiness of multiscale randomly rough surfaces. The journal of adhesion, 1-19.